Journal of Applied Physics ARTICLE scitation.org/journal/jap

Glide of threading dislocations in (In)AlGaAs on Si induced by carrier recombination: Characteristics, mitigation, and filtering

Cite as: J. Appl. Phys. **125**, 165702 (2019); doi: 10.1063/1.5088844
Submitted: 15 January 2019 · Accepted: 7 April 2019 ·
Published Online: 23 April 2019

Eamonn T. Hughes,[1,a)] Rushabh D. Shah,[2,a)] and Kunal Mukherjee[1,b)]

AFFILIATIONS

[1]Materials Department, University of California Santa Barbara, Santa Barbara, California 93106, USA
[2]Department of Materials Science and Engineering, Massachusetts Institute of Technology, Cambridge, Massachusetts 02139, USA

[a)]**Contributions:** E. T. Hughes and R. D. Shah contributed equally to this work.
[b)]**Author to whom correspondence should be addressed:** kunalm@ucsb.edu

ABSTRACT

III-V optoelectronics grown epitaxially on Si substrates have large networks of dislocations due to a lattice constant mismatch between the device layers and the substrate. Recombination-enhanced dislocation glide (REDG) allows these dislocations to move and increase in length during device operation, which degrades performance. In this paper, we study REDG dynamics of threading dislocations *in situ* in (In)AlGaAs double heterostructures grown on Si substrates using scanning electron microscopy cathodoluminescence. The driving force for REDG arises due to the coefficient of thermal expansion differences between Si and the III-V layers leading to large residual strains in the films. Tracking of threading dislocations as moving dark spot defects reveals glide characteristics that vary based on the nature of the dislocation. Remarkably, the alloying of a few atom percent of indium using metamorphic structures arrests threading dislocation glide by more than two orders of magnitude. Finally, we present REDG-based filtering as a pathway to reducing the threading dislocation density in select areas, removing a large fraction of the mobile dislocations. Together, these techniques will enable the understanding of dislocation–dislocation and carrier–dislocation interactions that have so far remained elusive during device operation, leading to reliable III-V integrated optoelectronics on silicon.

I. INTRODUCTION

The direct growth of optoelectronic semiconductors on silicon substrates is of great interest in the field of integrated photonics,[1–3] electronics,[4] and high efficiency photovoltaics.[5] Yet, such an approach has proved difficult due to large lattice constant mismatches between Si and workhorse III-V materials like GaAs and InP. The epitaxial growth of such lattice-mismatched semiconductors leads to the formation of dislocations—one dimensional crystal defects that degrade the electronic and optical properties of the material.[6] While misfit dislocations (MDs) at the interface between the film and the substrate are essential to relieving this lattice constant mismatch, these MDs have adjoining segments termed threading dislocations (TDs) that bend upwards into the device layers. These TDs are responsible for the poor reliability of heterogeneously integrated electronic devices such as GaAs-based lasers on Si, with the device performance degrading rapidly over time.[7] This degradation is fueled by large residual tensile strains of 0.15%–0.2% in the films at room temperature due to a mismatch in the coefficient of thermal expansion (CTE) between GaAs or Ge films (CTE = 5.7 and 5.9 ppm/K, respectively, at 300 K) and the Si substrate (CTE = 2.6 ppm/K at 300 K).[8] This large strain intensifies a remarkable class of processes known as recombination- or radiation-enhanced dislocation glide and climb (REDG and REDC) that result in rampant dislocation growth during device operation in these otherwise brittle materials.[9–11] These processes form part of the larger space of photoplastic effects in semiconductors relating to the strong coupling of electrical and mechanical properties of dislocations.[12,13]

We need to study the process of REDG and REDC of dislocations in III-V thin films on Si for reliable heterogeneous integration of optoelectronic devices. Normally, dislocations cannot move (glide or climb) at room temperature in GaAs due to high-energy barriers. Remarkably, some of the energy released during

nonradiative recombination at dislocations can assist the dislocation in surmounting these barriers, leading to the prefix "recombination-enhanced."[14,15] Here, both the initial barrier height and the extent of barrier lowering due to recombination depend on the type of dislocation. Most of our understanding of these important processes have come from the study of bulk crystals, but the density, character (line direction, Burgers vector, and core chemistry), and carrier recombination properties of TDs generated during heteroepitaxy on silicon is not like that generated by deformation or indentation in bulk crystals. Hence, characterizing REDG in samples with dislocation configurations similar to that in heteroepitaxial devices is important to understand failure mechanisms.

A few groups have noted that adding small amounts of indium in the active region of GaAs-based quantum well lasers impedes the formation of dislocation-related dark line defects.[16–18] There is debate over the mechanism for this. It is not clear if indium merely reduces the residual tensile strain in the active region or if there are additional metallurgical hardening effects at room temperature. In the latter case, different mechanisms could be at play from those seen in high temperature studies (>300 °C) of plasticity on bulk crystals.[19] Finally, there is some evidence from laser degradation studies that the presence of indium suppresses only REDC but not REDG;[20] this needs to be verified. Hence, a direct study of REDG at the single dislocation level in strain-controlled indium-containing samples would be useful to decouple the effects of competing phenomena.

In this work, we study the dynamics of REDG of TDs in (In)AlGaAs-based double heterostructures (DH) grown on Si using scanned cathodoluminescence (CL) intensity maps. Electron–hole pairs generated by the scanning electron beam induce REDG as they recombine nonradiatively at TDs. The residual strain in the epilayers arising from CTE mismatch provides the overall driving force for glide. We provide in this paper: (1) a description of the REDG behavior seen in AlGaAs heterostructures on Si, (2) a demonstration of strong reduction in REDG by adding a few percent of indium in carefully designed metamorphic samples, and (3) preliminary findings from an REDG-based dislocation-filtering experiment where we remove a large fraction of glissile TDs.

II. METHODS

We deposited our thin films on 150 mm silicon substrates offcut from [001] by 6° toward [$\bar{1}$11] to discourage antiphase domain formation.[21] This directional notation is consistent with the orientation of the subsequent III-V layers. First, a 1.2 μm layer of germanium was grown by an Epi Centura low pressure chemical vapor deposition (LPCVD) reactor using a two temperature step procedure.[22,23] These samples underwent five cycles of thermal annealing between 650 °C and 850 °C. Next, 150 nm of GaAs was grown in a Thomas Swan/Aixtron metalorganic chemical vapor deposition (MOCVD) reactor with a high AsH_3 overpressure.[24,25] These wafers were cleaved into smaller pieces and used as "prethreaded" substrates for subsequent (In)AlGaAs film growth.

Double heterostructures with an $In_x(Al_{0.15}Ga_{0.85})_{1-x}As$ active layer and $In_x(Al_{0.25}Ga_{0.75})_{1-x}As$ barriers were used for this study; x was chosen as 0 (indium-free), 0.02, and 0.05. Figure 1(a) shows the heterostructures layer design. We include a fourth sample in

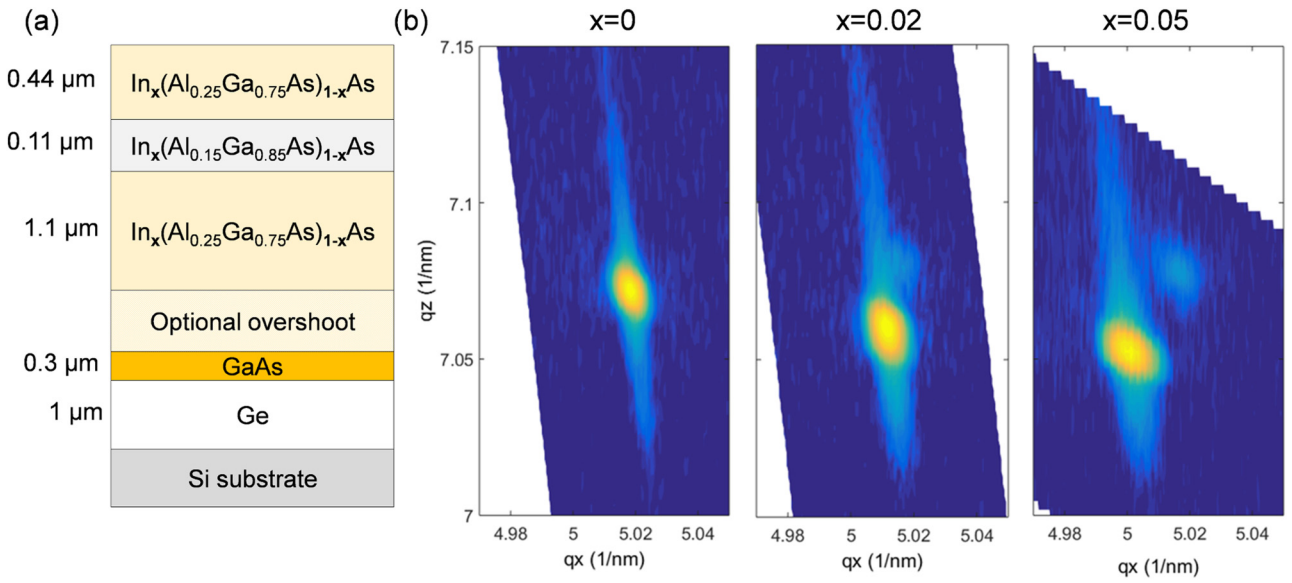

FIG. 1. (a) Layer structure of the arsenide heterostructures on silicon. The indium-free x = 0 sample is used for the detailed characterization of REDG in Sec. III A and filtering in Sec. III C. The indium containing x = 0.02 and x = 0.05 forms the basis of Sec. III B, where REDG is seen to be arrested. An overshoot layer is used for a second x = 0.05 sample to modify the residual strain. (b) A portion of the $\bar{2}24$ x-ray reciprocal space maps of the films for the compositions is indicated. The weaker peak seen in x = 0.02 and 0.05 corresponds to GaAs/Ge. We used larger scans that included the Si substrate peak to calculate the residual strain at room temperature. The sample with overshoot is not shown here.

our study also with x = 0.05 but with the addition of an overshoot layer. This layer provided fine control of the residual strain in the x = 0.05 (overshoot) heterostructure as is discussed subsequently. The films were grown at 725 °C with a V/III ratio of about 40 with H_2 as the carrier gas. The growth rates ranged from 1.0 to 1.4 nm/s, and the films were doped n-type $\approx 1 \times 10^{17}$ cm^{-3} using disilane. A 120 nm GaAs regrowth was performed on all samples before depositing (In)AlGaAs to reduce the effects of surface contamination from wafer cleaving and transfer. We ensure a similar starting dislocation density by growing the four DHs on "prethreaded" substrates. The thicknesses of the lower cladding, active layer and upper cladding layers are 1080 nm, 110 nm, and 440 nm, respectively, verified by transmission electron microscopy. After the growth of the upper cladding layer, we annealed these samples at the growth temperature for 300 s in the growth chamber to allow for maximum strain relaxation. A 3 nm thick capping layer of lattice-matched $In_xGa_{1-x}As$ was grown to prevent oxidation of the underlying Al-containing layers.

We measured the residual strain in our films using x-ray diffraction (XRD) using a Bruker D8 diffractometer with a Cu $K_{\alpha 1}$ radiation source and a linear array detector. Symmetric (004) and asymmetric ($\bar{2}24$) high-resolution (HR)-XRD reciprocal space maps (RSM) were collected and used to calculate the in-plane and out-of-plane lattice constant, while correcting for crystallographic tilt that may have developed during the growth.[26] Figure 1(b) shows the $\bar{2}24$ RSMs of the III-V layers for the three samples. The GaAs/Ge peak is distinct for the indium-containing films. Table I lists the measured residual tensile strain along the [$\bar{1}$10] direction. This strain is the net result of: (a) residual compressive strain after the high temperature processes (growth and subsequent anneal), (b) tensile strain due to integrated CTE mismatch, and (c) any strain relaxation of this tensile strain during cooldown. Uncertainty in the strain measurements is ±0.02%. The lower strain in the x = 0.05 sample is due to under-relaxation of compressive strain during growth. We compensated for this using the x = 0.05 (overshoot) sample using an overshoot layer of $In_{0.08}(Al_{0.15}Ga_{0.85})_{0.92}$ As (200 nm). We have confirmed that the residual strain in the [110] and [$\bar{1}$10] directions are within the uncertainty of the measurement technique for samples x = 0 and x = 0.05. While asymmetric strain relaxation in the [110] direction due to kinetic effects[27] can be important at moderate temperatures that occur during (c), this is expected to be insignificant for this study since the overall contribution of (c) is small because of the limited time and dislocation glide velocity.

We measured CL emission using an FEI Quanta 400F scanning electron microscope (SEM). The electron beam scan-rate parameters were chosen to match an image capture rate of one frame per second. We used a beam accelerating voltage of 5 kV for good dark spot defect resolution and contrast. Monte Carlo simulations using CASINO[28] show that the primary beam does not penetrate all the way into the DH active layer, however electron–hole pairs generated by the beam should easily be able to diffuse into the active layer. We estimate that the carrier concentration is around 10^{17} e-h pairs/cm^3. A mirror positioned directly above the sample directed the emitted light toward a photomultiplier tube sensitive up to about 870 nm. All CL data were taken at the same magnification, resolution, and dwell time to avoid unwanted artifacts due to the scanning nature of the probe, and we ensured that the area of interest was not exposed prior to imaging.

TABLE I. Measured residual strain.

Indium content (x)	Overshoot layer	Residual strain (tensile)
0	No	0.17%
0.02	No	0.16%
0.05	No	0.11%
0.05	Yes	0.16%

We surveyed large areas and counted clusters appropriately to measure average TD densities. We measured TD densities of 9.95×10^6 cm^{-2}, 1.65×10^7 cm^{-2}, 1.60×10^7 cm^{-2}, and 1.30×10^7 cm^{-2} with an uncertainty (2 sigma) $\approx 5 \times 10^5$ cm^{-2}, respectively, for samples x = 0, x = 0.02, x = 0.05, and x = 0.05 (overshoot). We measured the velocities of TDs by averaging the total distance traveled over a number of frames, with points manually chosen to ensure that the TDs were free from the influence of nearby defects. The CL contrast due to nonradiative recombination at the TDs was calculated as the positive difference in CL intensity between the TD and the bright background, normalized by the background intensity. Since no systematic or significant change in intensity was noted as the TDs moved, the CL intensity of the TDs was simply averaged from three points along the path of the moving TDs. For rapid analyses on this large dataset, we automated tracking of TDs using a single particle tracker as implemented in the Fiji plugin Trackmate.[29] Here, a Laplacian of Gaussian's method detects TDs as dark spots. Tracks were established by linking TD positions using the linear assignment problem (Simple LAP) tracker. Tracking is not yet effective near tight clusters and complex crossings, and, hence, the automated tracked images are used in a semiquantitative manner to provide an overall view of this phenomenon.

III. RESULTS AND DISCUSSION

A. REDG in AlGaAs heterostructures on Si

TDs in the indium-free (x = 0) AlGaAs heterostructures on Si are very clearly visible as dark spots in cathodoluminescence images, each with an average spot diameter of $\approx 1\,\mu$m when excited with a 5 kV beam. The CL contrast from dark spots is between 0.3 and 0.5 and relatively constant over 2 orders-of-magnitude change in probe current.

Repeated scans from the same area reveal that a number of TDs move by glide under the influence of the scanning electron beam, an effect we ascribe to REDG.[30,31] The driving force for REDG is the relief of tensile residual strain in the III-V layers. Importantly, we do not see a change in CL spot contrast during glide indicating that nonradiative recombination at TDs in these heterostructures is most likely intrinsic to the dislocation core as opposed to arising from an atmosphere of impurities.[32–34] Figures 2(a) and 2(b) show panchromatic CL emission intensity maps at the start and end, respectively, of a ≈2800 frame scan, taken at one frame per second using a 3 nA sample absorbed current (also in a video given in the supplementary material). A number of TDs have exited the area due to REDG and others have reorganized. Figure 2(c) presents an overall view of this phenomenon from the same area, with the tracked glide path of TDs

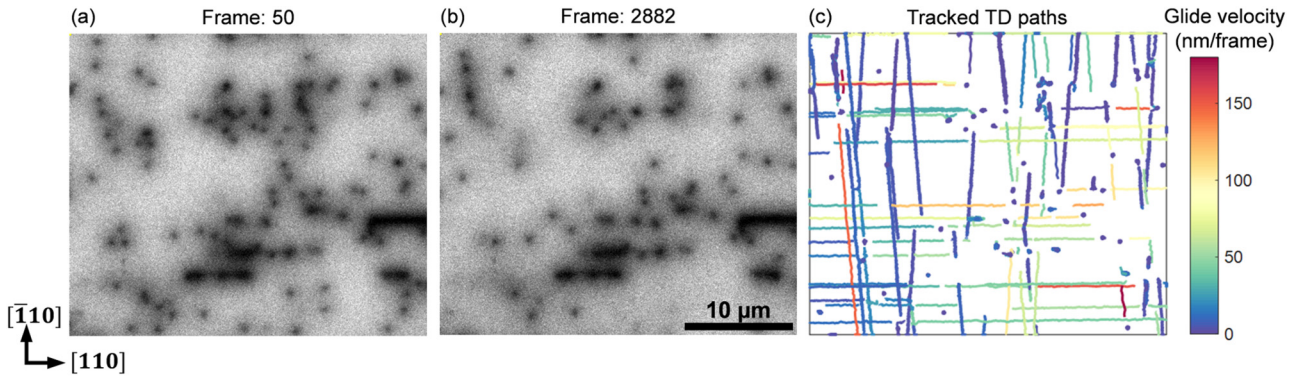

FIG. 2. Panchromatic cathodoluminescence emission from the AlGaAs (x = 0) heterostructure showing dark spots due to nonradiative recombination at threading dislocations. The images are taken with a 3 nA absorbed current and show the position of threading dislocations after (a) 50 frames and (b) 2882 frames (also in videos given in the supplementary material). A number of dislocations have exited the imaging area by REDG. (c) Tracks of the gliding TDs from the same area, colored by the glide velocity. Four types of dislocation behavior are seen: slow and fast motion along [$\bar{1}$10], fast motion along [110], and stationary dislocations. The inclined lines are due to the substrate offcut.

highlighted and the color of the path corresponding to the mean velocity (total displacement/total time). While glide velocities are normally in units of nm/s, we use nm/frame (1 frame captured every second) as the excitation is intermittent rather than continuous due to the scanning nature of the e-beam. We also do not see appreciable effects of the beam scan direction on the TD glide velocity. Finally, due to the substrate miscut, the intersection of the {111} TD glide planes and the substrate surface is no longer parallel and there are two families of MDs in the [$\bar{1}$10] direction that are slightly inclined to each other.[35] For all the discussion that follows in the paper, these slightly inclined directions are still referred to as TDs moving in the [$\bar{1}$10] direction.

1. General features

For the purposes of comparison between samples used in this study, we broadly categorize TD into one of four types depending on their velocities and temperature dependence: (1) slow and (2) fast dislocations, both gliding along the offcut direction of [$\bar{1}$10], (3) fast dislocations gliding along [110], and (4) dislocations that are stationary (within the detection limit). These types are seen best in Fig. 2(c). The ratio of the number of mobile and stationary dislocations is measured as near 1:1, an important data point concerning sessile and glissile TD densities that we will return to in Sec. III C. In the population of mobile TDs, the ratio of the number of fast [110], slow [$\bar{1}$10], and fast [$\bar{1}$10] TDs is approximately 2:2:1. As we have imaged a large number of TDs, we can look for correlations between the CL contrast and REDG velocity. Figure 3(a) shows this connection for the three types of mobile dislocations. The slow TDs have a measurably higher CL contrast in the range of 0.35–0.43 compared to both sets of fast TDs that exhibit contrast between 0.3 and 0.36. Yet in the class of fast TDs, we find no change in the CL contrast for an order-of-magnitude range of velocity. We think that CL contrast and REDG velocity are uncorrelated within a given type of TD, but there might be a link between nonradiative recombination and the type of TD. Interestingly, we do not see ⟨110⟩ dark line defects in the CL images that should form due to the glide of the upper parts of TDs forming MD segments. We think that the MDs form at some depth below the active layer of the double heterostructure in a self-regulating manner where the excess carrier concentration is very low. This process enables relatively unimpeded glide of TDs leading to smooth glide motion.

2. Temperature dependence

We probe the energetics of the REDG process in TDs by measuring glide velocities at temperatures from −20 °C to 60 °C, typical for device operation. Figure 3(b) shows the REDG velocity as a function of inverse temperature for the three-mobile types of dislocations. We do see an increase in TD glide velocity with increasing temperature for the fast TDs. The operation of REDG is approximately 50%–100% faster at 60 °C compared to room temperature. The CL contrast of the TDs does not change in this temperature range, suggesting no change in the nonradiative recombination mechanism. Assuming that the TD velocity v follows a simple Arrhenius form $v \propto e^{(-E_a/kT)}$,[36] we measure very small activation energies E_a of 0.16 eV and 0.08 eV for the glide of fast TDs along [110] and [$\bar{1}$10], respectively. The velocity of the slow TDs along [$\bar{1}$10] did not exhibit a well-behaved temperature dependence in the limited temperature range, so we could not obtain an activation energy. It is presently unclear why this happens. Finally, we note that we are altering the strain state slightly by varying the temperature since the strain in these films is due to a thermal expansion mismatch. This counteracts the changes in velocity from temperature alone. Correcting for this effect using a stress–velocity relation for α-dislocations from Maeda *et al.*,[37] only slightly larger activation energies of 0.17 eV and 0.10 eV are found.

Here, we also note that due to the offcut substrate, the resolved shear stress varies among the set of active slip planes by around 17%. While this contributes to the spread of measured velocities in both directions, it cannot entirely explain the spread of measured velocities evident in Fig. 3.

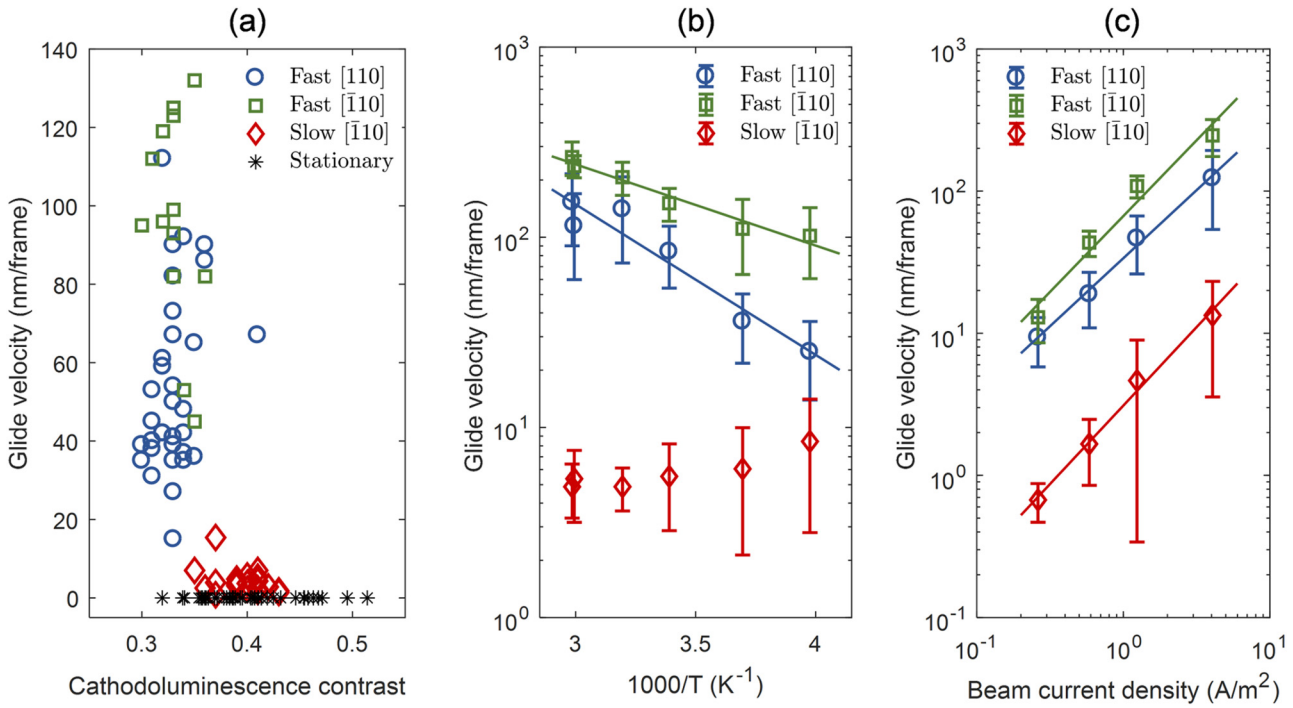

FIG. 3. (a) Relationship between cathodoluminescence contrast due to nonradiative recombination and the corresponding REDG velocity. The sample absorbed current is 1 nA. (b) Temperature dependence of REDG velocity showing very low activation energies for the fast dislocations. The sample absorbed current is 1.5 nA. The slow dislocation glide velocity does not show appreciable temperature dependence. (c) Beam current dependence of REDG velocity showing a nearly linear dependence.

3. Beam current dependence

Figure 3(c) shows the dependence of REDG on the carrier injection level. Here too, we note that the CL contrast of TDs remains similar for all levels of injection. The TD glide velocity is linearly dependent on the current for all types of TDs. Maeda *et al.* see similar linear behavior in dislocations in bulk GaAs, which they say arises due to a diffusive carrier flux to the dislocation that is proportional to the excess generated electron–hole pairs.[37] This linear beam current dependence of REDG velocity also provides insight into the microscopic mechanism of enhanced TD glide. In the diffusive kink model of dislocation glide, the activated processes of kink-pair formation and kink migration control the glide velocity. Maeda *et al.* have shown that a linear dependence of REDG velocity on current injection implies that nonradiative recombination enhances kink-pair formation at the very least.[15] It is much more challenging to verify if nonradiative recombination also enhances kink migration as this depends on whether the TD glides in a kink-collision or kink-collisionless regime. This can be the subject of future work where samples of different TD segment lengths can be probed.

4. Comparison with prior measurements of REDG in bulk GaAs crystals

The differences in mobilities and CL contrast between TDs that we have seen are very likely due to differences in structures and core-chemistries of the dislocation, analogous to reports in bulk crystals.[38] Yet, due to complexities in the nature of TDs, a definitive assignment of a TD type cannot be made by comparing to REDG behavior in bulk crystals. Briefly, dislocations in the glissile-set in bulk GaAs with 110 line directions are categorized as α-type (As-core), β-type (Ga-core), and screw-type. Each dislocation type has a different REDG velocity and activation energy that also depends on doping.[38] Simply extrapolating bulk crystal REDG measurements of isolated dislocations to room temperature, α-type dislocations should have REDG velocities five orders-of-magnitude higher than β-type dislocations and three orders-of-magnitude higher than screw dislocations. We do not see such a drastic difference in velocities among TDs in this study. The velocity ratio is 1–1.5 orders-of-magnitude between fast and slow TDs along [$\bar{1}$10] at room temperature. Additionally, fast TDs in the two orthogonal directions have different activation energies that are both lower than that reported in bulk GaAs crystals. This prevents an assignment of core type to the measured data based on prior literature.

In lattice-mismatched films, the character of MDs is well defined. For example, tensile strain in GaAs is relieved by 60°(α) MDs along [110] and 60°(β) MDs along [$\bar{1}$10]. In contrast, the core structure of a TD does not have such a unique configuration for a given sense of strain. The most commonly discussed orientation of the two TDs attached to a MD in a half-loop is one where the TDs lie along out-of-plane ⟨011⟩ directions with obtuse angles to the corresponding MDs, resulting in one set of possible TD core types.

However, arguments have been made for the existence of a reverse 60° TD configuration, i.e., a TD that makes an acute angle with a MD,[39,40] resulting in a different combination of core types of TDs associated with a given MD. This possibility prevents an assignment of TDs solely based on their direction of motion. Additionally, to minimize line tension during film growth, TDs may not be of pure screw or 60° type as described above but instead have an average line direction such as ⟨112⟩ and ⟨123⟩.[41] TEM images of nonstraight TD segments are common in the literature. Lastly, impurities at the dislocation core are expected to be different for grown-in dislocations in the epitaxial films as compared to those created by mechanical deformation. Such differences in the core can change the nonradiative recombination properties at defects associated with the dislocation and hence have a significant impact on REDG velocity and its activation energy. Due to the several possible configurations of TDs discussed above, we cannot determine the core type of the TDs with REDG data alone; further study of REDG in heteroepitaxial systems using advanced transmission electron microscopy is required.[42,43]

B. Metamorphic indium-containing heterostructures

We now consider the effect of alloying ≈2% and 5% indium in the entire heterostructure to probe its effect on REDG. Here, indium is introduced via metamorphic structures ensuring that the films remain in a state of tension at room temperature. This would not have been the case in more conventional compressively strained (pseudomorphic) InGaAs quantum wells, where the addition of indium reduces/negates CTE-mismatch induced tension. As a reminder, the residual tensile strains in our samples are $\varepsilon = 0.16\%$ for $x = 0.02$ and slightly lower at $\varepsilon = 0.11\%$ for $x = 0.05$. As strain influences glide velocity, we also study $x = 0.05$ (overshoot) where the strain is increased back up to $\varepsilon = 0.16\%$.

We find that the addition of indium in the heterostructure dramatically reduces the REDG velocities of all TDs, seen in Fig. 4 (also in videos given in the supplementary material). At the same time, the CL contrast at TDs is unaffected. In the $x = 0.02$ indium alloy [Fig. 4(a)], only a quarter of the TDs can be characterized as moving, with about three times more TDs gliding along the [110] compared to the [$\bar{1}$10]. Looking at the maximum TD velocities, the presence of 2% indium reduces REDG along [110] by a factor of 20–30 compared to the indium-free heterostructure. It is notable that the glide of the TDs remains smooth and continuous as in the indium-free sample. The total length of TD glide reduces by more than two orders of magnitude. This is significant for device reliability, as REDG-formed MD segments not only act as immediate nonradiative sites but also as sites for REDC.

Increasing the indium content to $x = 0.05$ practically stops all TD motion as seen in Fig. 4(b). As part of this reduction is due to the lower residual strain, we also compare to the $x = 0.05$ indium sample with the overshoot layer. In this sample [Fig. 4(c)], less than a tenth of all TDs glide and all of them do so along the [110] with lower velocities than those of the $x = 0.02$ sample. The total MD length is further reduced to only half that of the $x = 0.02$ sample. In summary, we have shown that alloying indium via metamorphic heterostructures significantly reduces REDG by lowering both the fraction of mobile dislocations and their velocities. We have shown this while controlling for the CTE-induced residual tensile strain.

Let us now consider different mechanisms that can explain the decrease in REDG velocity. We can straightaway rule out decreased carrier recombination at the TD based on the CL contrast, which is quite similar to the indium-free samples. Slowing due to pinning of TDs at the MD network between GaAs and InAlGaAs is also unlikely as the film is thick.[44] Any pinning strain at that interface would decay rapidly only slightly above the interface, leaving sufficient driving force for TD glide. Prior results[45] on atom probe tomography (APT) at single dislocations in InGaAs layers grown similarly do not provide clear evidence of local segregation at the core as suggested by Kirkby.[46] Other groups have proposed another form of core segregation where interstitial indium migrates to shuffle sites only on the α-type partial cores, leading to preferential slowing of α-type or screw dislocations.[47,48] While such segregation would be undetectable by APT, it seems unlikely that nonradiative recombination could dynamically move interstitial indium atoms as the dislocation glides. Even if this were possible, this would indicate

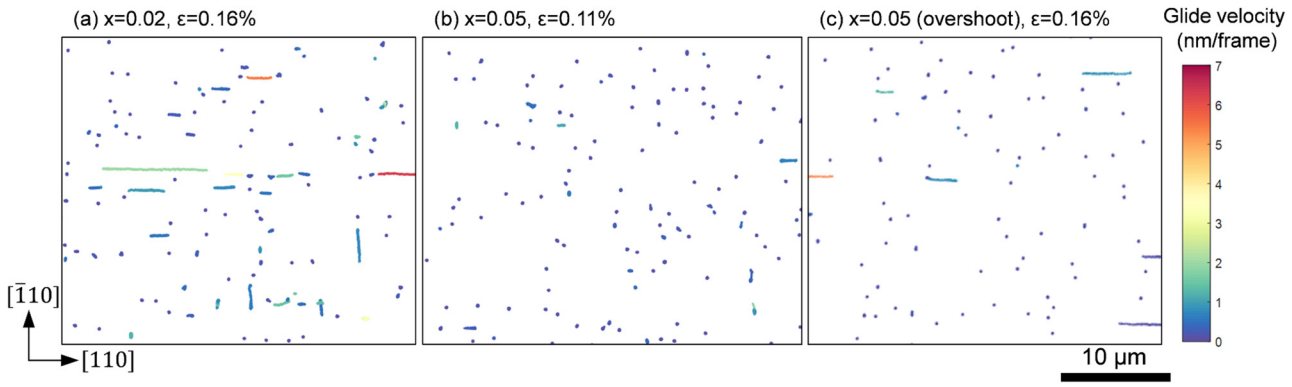

FIG. 4. Tracks of threading dislocations undergoing recombination-enhanced glide colored by their velocity (also in videos given in the supplementary material). The samples (and the number of frames) are $x \approx 0.02$ (2100), $x = 0.05$ (1600), and $x = 0.05$ (2100) with the overshoot layer. The residual strain is also listed. A sample absorbed current of ≈3 nA is used. The dislocation glide velocity clearly reduces upon the addition of indium and a majority of dislocations are stationary.

that TDs should glide progressively slower the farther they travel as they accumulate In in their cores,[47] a trend we do not see. This leaves solute hardening first proposed by Ehrenreich and Hirth[49] as the likely mechanism. Here, the hardening agent is actually the $InAs_4$ tetrahedron, which is 21% larger in volume than the $GaAs_4$ tetrahedron,[50] and the strain field around such fixed centers could slow down the migration of kinks along the dislocation. Higher indium concentrations would result in a greater number of such obstacles and hence a lower glide velocity. What remains unexplained is the asymmetry in reduction of REDG along [110] and [$\bar{1}$10]. We can rule out strain effects as the metamorphic buffer is relaxed uniformly in these two orthogonal directions as measured by XRD. It remains to be seen if such an asymmetric reduction in velocity could arise due to the impact of core chemistry and line directions on solute hardening.[47]

In summary, we have shown that metamorphic structures containing indium have very significantly reduced REDG, most likely a result of solute hardening. Importantly, such a hardening mechanism is not limited to REDG. It could also reduce potential thermal glide during strain relief at higher temperatures involved in growth, subsequent cool down, and during device processing. This opens the possibility of employing lattice hardening to alleviate misfit line defects seen in the recent work on III-V lasers on Si.[51]

C. Prospects for dislocation filtering

The existence of REDG in III-V materials on Si presents the intriguing prospect of recombination-enhanced filtering of TDs using excitation sources such as light, electron beams, or even current injection. Naturally, such a technique would be most useful in patterned mesa regions where the TD can exit at the free edges. To quantify the efficacy of such a filter in the x = 0 indium-free sample, we present results from an automated count of the TDs in the e-beam exposed region as a function of time in Fig. 5. The starting TD density is $\approx 1 \times 10^7\ cm^{-2}$. Here, the TDs simply glide out of the imaged area until the carrier recombination stops. We observe an initial rapid increase in the TD density of around 20% followed by a decline. This initial rise is caused by the ungrouping of closely spaced TDs that could not be individually distinguished. Once, the TDs are sufficiently separated, a total decline from the highest TD count of about 30% is measured after 40 min of scanning e-beam exposure involving two stages of reduction. A sharp decline in count occurs for the first 300 frames corresponding to the fast TDs gliding out of the imaging area (an average glide velocity of 100 nm/frame). A slower second stage of TD density decline follows, corresponding to slower TDs gliding out of the area. At the end of the measurement, the sample is yet to reach steady state, with some TDs still moving in the frame.

Since REDG only impacts glissile dislocations, the efficacy of such a filter depends primarily on the fraction of TDs that are glissile. Ward *et al.* estimate a steady state fraction of glissile dislocations to be 50% for face-centered cubic semiconductors like GaAs, based on continued interactions between populations of glissile and sessile dislocations during heteroepitaxy.[52] Knall *et al.* reported the fraction of glissile dislocations as two thirds for InGaAs films on thermal cyclically annealed GaAs/Si templates.[53] Thus, a REDG-based filter could theoretically remove up to 66% of TDs—significant for metamorphic minority carrier devices as conventional efforts to reduce

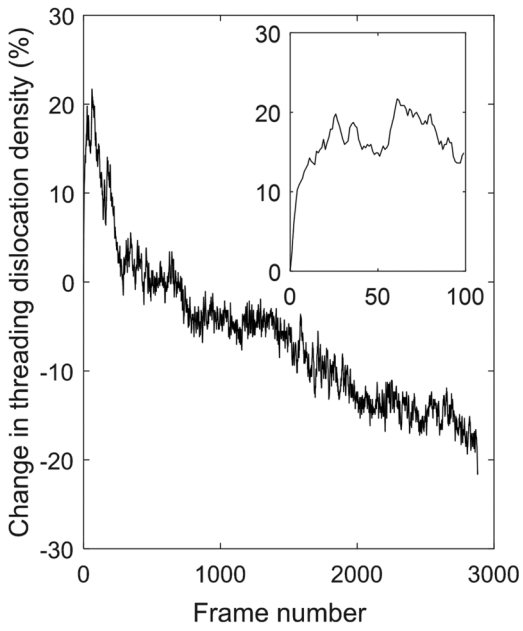

FIG. 5. The efficacy of a recombination-enhanced glide-based dislocation filter. The change in the threading dislocation density in a 1000 μm^2 area is shown as a function of frames (time) for a sample absorbed current of ≈3 nA. The starting dislocation density is $\approx 1 \times 10^7\ cm^{-2}$. The inset shows the apparent increase in the dislocation density in the first 100 frames due to declustering of TDs.

dislocation densities approach practical limits. However, our results show that a complete removal of glissile dislocations might not be possible. We see that some slow TDs are attracted to TD super structures resembling subgrain boundaries previously noted in bulk GaAs wafers.[54] We also see the sporadic appearance of new TDs and TD-pairs throughout the excitation process either from existing TDs (which do not appear to be initially clustered) or appear into existence from CL-invisible sources deeper in the metamorphic buffer. Such sources and reaction events, respectively, increase and decrease dislocation density by a small amount (<5%) and will be discussed in a subsequent study. In summary, REDG-based filtering is very capable of removing the fastest glissile TDs that are arguably the more damaging to optoelectronic devices. We advise the use of such filtering only after reaction-based filtering reaches a limit as the treated area is rendered largely devoid of glissile dislocations that are necessary for further annihilation/fusion events.[52] Future work with this technique will focus on understanding TD pinning and TD sources, interactions that also likely limit conventional growth-based defect filters.

IV. CONCLUSIONS

With continuing progress toward heterogeneous integration of III-V devices on silicon, future commercial applications necessitate a study of how dislocations in such devices respond to carrier injection. Such insight will be useful for engineering heterostructures with degradation tolerance and in constructing failure analysis

models. We use an AlGaAs-based double heterostructure epitaxially grown on Si as a model system to study REDG at the level of individual TDs. The motion of dark spots in the cathodoluminescence signal shows that the unique structure of TDs in films on silicon leads to REDG behavior that is distinct from that in bulk crystals. The addition of a few percent of indium reduces REDG by two orders of magnitude at room temperature, essentially freezing the motion of dislocations. After controlling for the residual strain using metamorphic structures, we think this effect is most likely due to solute hardening. Future work will involve studying such metallurgical effects on REDG and REDC in devices like quantum dot lasers on silicon. Our dislocation-tracking approach also provides an experimentally convenient method to learn about the various populations of TDs types generated during III-V growth on silicon. Using this, we show that REDG itself removes glissile TDs from an area quite effectively and has potential as a dislocation-filtering tool. Better statistics on dislocation populations is now more important than ever to make continued improvements in defect density and reliability, and our paper outlines techniques for this.

SUPPLEMENTARY MATERIAL

Four panchromatic CL movies used to create Figs. 2, 4, and 5 taken at 1 frame/s are given in the supplementary material. The horizontal direction is the [110]. The accelerating voltage was 5 kV and the sample absorbed current was 3 nA. The filenames refer to the samples, x = 0, x = 0.02, x = 0.05, and x = 0.05 (overshoot). The videos play at 60 frames/s and have the contrast enhanced to show TDs more clearly.

ACKNOWLEDGMENTS

This work was partially supported by the MRSEC Program of the National Science Foundation under Award No. DMR 1720256 at UCSB. The x-ray characterization made use of the MRSEC Shared Experimental Facilities at MIT, supported by the National Science Foundation under Award No. DMR 1419807.

REFERENCES

[1]A. Y. Liu, C. Zhang, J. Norman, A. Snyder, D. Lubyshev, J. M. Fastenau, A. W. K. Liu, A. C. Gossard, and J. E. Bowers, Appl. Phys. Lett. **104**, 041104 (2014).
[2]D. Thomson, A. Zilkie, J. E. Bowers, T. Komljenovic, G. T. Reed, L. Vivien, D. Marris-Morini, E. Cassan, L. Virot, J.-M. Fédéli, J.-M. Hartmann, J. H. Schmid, D.-X. Xu, F. Boeuf, P. O'Brien, G. Z. Mashanovich, and M. Nedeljkovic, J. Opt. **18**, 073003 (2016).
[3]S. Chen, W. Li, J. Wu, Q. Jiang, M. Tang, S. Shutts, S. N. Elliott, A. Sobiesierski, A. J. Seeds, I. Ross, P. M. Smowton, and H. Liu, Nat. Photonics **10**, 307 (2016).
[4]B. Kunert, Y. Mols, M. Baryshniskova, N. Waldron, A. Schulze, and R. Langer, Semicond. Sci. Technol. **33**, 093002 (2018).
[5]R. M. France, F. Dimroth, T. J. Grassman, and R. R. King, MRS Bull. **41**, 202 (2016).
[6]E. A. Fitzgerald, Mater. Sci. Rep. **7**, 87 (1991).
[7]O. Ueda, Jpn. J. Appl. Phys. **49**, 090001 (2010).
[8]G. F. Burns and C. G. Fonstad, IEEE Photonics Technol. Lett. **4**, 18 (1992).
[9]B. Monemar, Phys. Scr. **24**, 367 (1981).
[10]Z. I. Kazi, P. Thilakan, T. Egawa, M. Umeno, and T. Jimbo, Jpn. J. Appl. Phys. **40**, 4903 (2001).
[11]M. E. Groenert, C. W. Leitz, A. J. Pitera, V. Yang, H. Lee, R. J. Ram, and E. A. Fitzgerald, J. Appl. Phys. **93**, 362 (2003).
[12]Y. A. Osip'yan, V. F. Petrenko, A. V. Zaretskiĭ, and R. W. Whitworth, Adv. Phys. **35**, 115 (1986).
[13]S. Koubaiti, J. J. Couderc, C. Levade, and G. Vanderschaeve, Mater. Sci. Eng. A **234–236**, 865 (1997).
[14]P. Petroff and R. L. Hartman, J. Appl. Phys. **45**, 3899 (1974).
[15]K. Maeda, Y. Yamashita, N. Maeda, and S. Takeuchi, MRS Online Proc. Libr. Arch. **184**, 69 (1990).
[16]S. L. Yellen, A. H. Shepard, R. J. Dalby, J. A. Baumann, H. B. Serreze, T. S. Guido, R. Soltz, K. J. Bystrom, C. M. Harding, and R. G. Waters, IEEE J. Quantum Electron. **29**, 2058 (1993).
[17]R. F. Murison, A. H. Moore, N. Holehouse, and S. R. Lee, Proc. SPIE **1850**, 215 (1993).
[18]Y. Hasegawa, T. Egawa, T. Jimbo, and M. Umeno, Jpn. J. Appl. Phys. **35**, 5637 (1996).
[19]I. Yonenaga and K. Sumino, J. Appl. Phys. **62**, 1212 (1987).
[20]J. J. Coleman, R. G. Waters, and D. P. Bour, Proc. SPIE **1418**, 318 (1991).
[21]S. M. Ting and E. A. Fitzgerald, J. Appl. Phys. **87**, 2618 (2000).
[22]H.-C. Luan, D. R. Lim, K. K. Lee, K. M. Chen, J. G. Sandland, K. Wada, and L. C. Kimerling, Appl. Phys. Lett. **75**, 2909 (1999).
[23]O. O. Olubuyide, D. T. Danielson, L. C. Kimerling, and J. L. Hoyt, Thin Solid Films **508**, 14 (2006).
[24]D. Kohen, S. Bao, K. H. Lee, K. E. K. Lee, C. S. Tan, S. F. Yoon, and E. A. Fitzgerald, J. Cryst. Growth **421**, 58 (2015).
[25]T. J. Milakovich, "Integration of GaAsP alloys on Si for high-efficiency III-V/Si PV," Ph.D. thesis, Massachusetts Institute of Technology, 2015.
[26]T. Roesener, V. Klinger, C. Weuffen, D. Lackner, and F. Dimroth, J. Cryst. Growth **368**, 21 (2013).
[27]I. Yonenaga and K. Sumino, J. Cryst. Growth **126**, 19 (1993).
[28]H. Demers, N. Poirier-Demers, A. R. Couture, D. Joly, M. Guilmain, N. de Jonge, and D. Drouin, Scanning **33**, 135 (2011).
[29]J.-Y. Tinevez, N. Perry, J. Schindelin, G. M. Hoopes, G. D. Reynolds, E. Laplantine, S. Y. Bednarek, S. L. Shorte, and K. W. Eliceiri, Methods **115**, 80 (2017).
[30]K. Maeda and S. Takeuchi, Jpn. J. Appl. Phys. **20**, L165 (1981).
[31]P. G. Callahan, B. B. Haidet, D. Jung, G. G. E. Seward, and K. Mukherjee, Phys. Rev. Mater. **2**, 081601 (2018).
[32]A. Djemel, J. Castaing, N. Visentin, and M. Bonnet, Semicond. Sci. Technol. **5**, 1221 (1990).
[33]M. Albrecht, J. L. Weyher, B. Lucznik, I. Grzegory, and S. Porowski, Appl. Phys. Lett. **92**, 231909 (2008).
[34]K. Mukherjee, C. H. Reilly, P. G. Callahan, and G. G. E. Seward, J. Appl. Phys. **123**, 165701 (2018).
[35]P. Kightley, P. J. Goodhew, R. R. Bradley, and P. D. Augustus, J. Cryst. Growth **112**, 359 (1991).
[36]B. W. Dodson and J. Y. Tsao, Appl. Phys. Lett. **51**, 1325 (1987).
[37]K. Maeda, M. Sato, A. Kubo, and S. Takeuchi, J. Appl. Phys. **54**, 161 (1983).
[38]K. Maeda and S. Takeuchi, J. Phys. Colloques **44**, C4 (1983).
[39]G. P. Watson, M. O. Thompson, D. G. Ast, A. Fischer-Colbrie, and J. Miller, J. Electron. Mater. **19**, 957 (1990).
[40]R. S. Goldman, K. L. Kavanagh, H. H. Wieder, S. N. Ehrlich, and R. M. Feenstra, J. Appl. Phys. **83**, 5137 (1998).
[41]A. E. Romanov, W. Pompe, G. Beltz, and J. S. Speck, Phys. Status Solidi B **198**, 599 (1996).
[42]S. Lopatin, S. J. Pennycook, J. Narayan, and G. Duscher, Appl. Phys. Lett. **81**, 2728 (2002).
[43]X. Xu, S. P. Beckman, P. Specht, E. R. Weber, D. C. Chrzan, R. P. Erni, I. Arslan, N. Browning, A. Bleloch, and C. Kisielowski, Phys. Rev. Lett. **95**, 145501 (2005).
[44]V. T. Gillard, W. D. Nix, and L. B. Freund, J. Appl. Phys. **76**, 7280 (1994).
[45]B. Bonef, R. D. Shah, and K. Mukherjee, Nano Lett. **19**, 1428 (2019).
[46]P. A. Kirkby, IEEE J. Quantum Electron. **11**, 562 (1975).
[47]F. Louchet, J. Phys. France **49**, 1219 (1988).
[48]N. Burle-Durbec, B. Pichaud, and F. Minari, Philos. Mag. Lett. **59**, 121 (1989).

[49]H. Ehrenreich and J. P. Hirth, Appl. Phys. Lett. **46**, 668 (1985).
[50]J. C. Mikkelsen and J. B. Boyce, Phys. Rev. B **28**, 7130 (1983).
[51]D. Jung, J. Norman, Y. Wan, S. Liu, R. Herrick, J. Selvidge, K. Mukherjee, A. C. Gossard, and J. E. Bowers, Physica Status Solidi A **216**, 1800602 (2019).
[52]T. Ward, A. M. Sánchez, M. Tang, J. Wu, H. Liu, D. J. Dunstan, and R. Beanland, J. Appl. Phys. **116**, 063508 (2014).
[53]J. Knall, L. T. Romano, D. K. Biegelsen, R. D. Bringans, H. C. Chui, J. S. Harris, Jr., D. W. Treat, and D. P. Bour, J. Appl. Phys. **76**, 2697 (1994).
[54]A. K. Chin, A. R. von Neida, and R. Caruso, J. Electrochem. Soc. **129**, 2386 (1982).